IOP Publishing Journal of Physics D: Applied Physics
J. Phys. D: Appl. Phys. **53** (2020) 435201 (7pp) https://doi.org/10.1088/1361-6463/ab9f68

# Influence of metastable atoms in low pressure magnetized radio-frequency argon discharges

**Bocong Zheng[1], Yangyang Fu[2,3], De-qi Wen[2,3], Keliang Wang[1], Thomas Schuelke[1,3] and Qi Hua Fan[1,3,4,5]**

[1] Fraunhofer Center for Coatings and Diamond Technologies, Michigan State University, East Lansing, MI 48824, United States of America
[2] Department of Computational Mathematics, Science and Engineering, Michigan State University, East Lansing, MI 48824, United States of America
[3] Department of Electrical and Computer Engineering, Michigan State University, East Lansing, MI 48824, United States of America
[4] Department of Chemical Engineering and Materials Science, Michigan State University, East Lansing, MI 48824, United States of America

E-mail: bzheng@fraunhofer.org and qfan@egr.msu.edu

Received 16 April 2020, revised 5 June 2020
Accepted for publication 23 June 2020
Published 30 July 2020

**Abstract**

One-dimensional particle-in-cell simulations with Monte Carlo collisions are used to investigate the influence of metastable atoms in low pressure radio-frequency argon discharges with magnetic fields ranging from 0 G to 60 G. Two metastable levels of argon species are included and tracked as particles, enabling multistep ionization and metastable pooling. At low magnetic fields, the metastable argon atoms have little influence on the discharge. At higher magnetic fields, the electron density increases and the electron temperature decreases at the center of the discharge with the inclusion of metastable atoms. The reduction in electron temperature is attributed to the depletion of energetic electrons due to low-energy-threshold reactions related to the metastable atoms. The reduced electron temperature leads to a reduction in the total ionization rate, albeit the contribution of multistep ionization increases with the magnetic field. The suppression of plasma diffusion at low electron temperatures plays a greater role than the reduction in ionization rate, resulting in a higher electron density. A transformation in metastable density profiles from parabolic to saddle type is observed with the increase in the magnetic field. Metastable atoms may play an important role in modulating the electron temperature in low pressure magnetized discharges.

Keywords: capacitively coupled plasma, particle-in-cell simulation, magnetic field, metastable atoms

(Some figures may appear in colour only in the online journal)

## 1. Introduction

Low pressure, magnetized radio-frequency (RF) plasmas are widely used for material processing [1]. Radio-frequency magnetron sputtering (RFMS) [2] and magnetic field enhanced capacitively coupled plasma reactors [3] are among the most commonly used magnetized sources. A static magnetic field applied parallel to the electrodes can appreciably confine the motion of electrons, reduce the rate of electron loss along the electric field, thereby achieving a high plasma density at relatively low pressures.

[5] Author to whom any correspondence should be addressed.

 

Apart from the high plasma density, a significant difference in the discharge characteristics is also observed in low pressure magnetized RF plasmas. A small transverse magnetic field of 10 G can induce a heating mode transition from a stochastic-heating dominated state to an Ohmic-heating dominated state [4], for the discharge is confined by the magnetic field and becomes a local regime, causing an increase in Hall current in the $\boldsymbol{E} \times \boldsymbol{B}$ direction [5]. With magnetic fields, a transition in the shape of electron energy probability function (EEPF) is observed, from a bi-Maxwellian type in the absence of a magnetic field, to a Maxwellian type at low magnetic field of 10 G [6], and a Druyvesteyn type at higher magnetic fields up to dozens of Gauss [5, 7], due to an enhancement of the plasma collisionality and a suppression of the nonlocal electron motion which causes the EEPF grouping.

In addition to charged species and neutrals, there are long-lived metastable atoms in the discharge. These metastable atoms are primarily produced through electron-impact excitation from ground state, which is an important path for the electron energy dissipation. However, the metastable atoms could also be an important ionization source and have a significant influence on the EEPF due to the relatively large cross sections and low threshold energies of electron-metastable collision reactions. For atmospheric pressure plasmas, the generation and modulation of reactive particle species is of great interest in the field of plasma medicine [8]. Recent investigations on micro atmospheric helium RF plasma jets [9] have shown that the density of helium metastables can be modulated by voltage waveform tailoring, through its controlling effect on the EEPF. Previous fluid simulations have shown that, at 1 Torr, the electron density peaks in the central bulk and metastable atom density peaks near the plasma sheath interface [10]. By including the metastables, the plasma density is significantly influenced and increased by one order of magnitude [11]. Particle-in-cell (PIC) simulations have also shown that, at relatively high pressures of up to 1 Torr, the multi-step ionization and the metastable pooling contribute a significant percentage to the total ionization rate and strongly influence the electron heating; however, at a relatively low pressure of 50 mTorr, the metastable atoms have little influence on the RF argon discharges [12, 13].

In practical applications, reactive species with complicated chemistries are often adopted to achieve various purposes [14], and the discharge dynamics can be significantly influenced. Albeit there have been many simulation and experimental investigations on the influence of metastable atoms on RF discharges under various pressures and frequencies [12, 13, 15–21], there exist few studies investigating the influence of metastable atoms on low-pressure magnetized plasmas. However, the fluid model breaks down for low pressure magnetized plasmas due to the expected strong deviations from equilibrium. The energy distributions of electrons as well as other species are no longer Maxwellian and the description of plasma behavior by averaged statistical properties becomes invalid.

This work aims to gauge the effects of metastable atoms on low-pressure magnetized plasma discharges. We address this issue by means of one-dimensional PIC simulations with Monte Carlo collisions. The PIC simulation, although computationally expensive, contains no assumptions about the electron energy distribution function, therefore provides detailed information on plasma kinetics. The simulation is performed in a symmetric capacitively coupled plasma reactor with an electrode separation of 5 cm. The applied voltage, the driving frequency, and the gas pressure are kept constant at 100 V, 15 MHz, and 10 mTorr, respectively. The influence of magnetic field on the electron density and temperature, the EEPF, the ionization rates as well as the profiles of metastable densities are examined.

## 2. PIC simulations

The numerical calculations are based on our ASTRA PIC/Monte Carlo collision simulation code (see the description in the supplementary material of [5]), which can choose to use an implicit algorithm to speed up the calculation. To simplify the analysis, no external circuit is considered, the secondary electron emission and electron reflection coefficients at the electrodes are assumed to be 0. Four species are tracked in the simulation, the electrons e, the argon ions $Ar^+$, and two lumped excited states of argon, i.e. the first excited state $Ar(3p^5 4s)$ and the next higher excited state $Ar(3p^5 4p)$, hereinafter referred to as Ar(4s) and Ar(4p). Metastable atoms, created through collisions with electrons, diffuse through the discharge and interact with neutral and charged species. Different particle weights, i.e. the ratio of the number of real particles to computational superparticles, are assigned to different species to alleviate the computational load. The collision of particles with different weights follow the implementation in oopd1 [22] to ensure that momentum is conserved. The ground state argon, is uniformly distributed in space with a temperature of 300 K. The reactions used here are listed in table 1 the corresponding cross sections are demonstrated in figure 1. Other de-excitation processes, such as spontaneous emissions, have been proved to be relatively unimportant [13, 21] and are not considered here. The argon chemistry set include these two metastable levels makes it possible to consider the multi-step ionizations (reactions (9) and (10)) and the metastable pooling (reaction (13)). The initial uniform number density of each tracked species, i.e. the electrons e, the argon ions $Ar^+$, and the excited states of argon Ar(4s) and Ar(4p), is $10^{14}$ $m^{-3}$. For all simulation results, we adopted an implicit algorithm and an energy conservation scheme, with 100 grid points and 800 time steps per rf period. These conditions satisfy the convergence conditions and benchmarks can be found in the supplementary material of [5]. The simulations were performed until the plasma achieved a steady state, typically required simulating on the order of 1 to 3 milliseconds depends on conditions.

The one-dimensional model used here and in previous studies [4–7] only considers the plasma diffusion loss parallel to the electric field. However, the transport and loss of electrons along the magnetic field as well as along the $\boldsymbol{E} \times \boldsymbol{B}$ direction may be dominant in practical applications where the magnetic field is high. Hence, the effect of magnetic field is overestimated in one-dimensional simulations. Here,

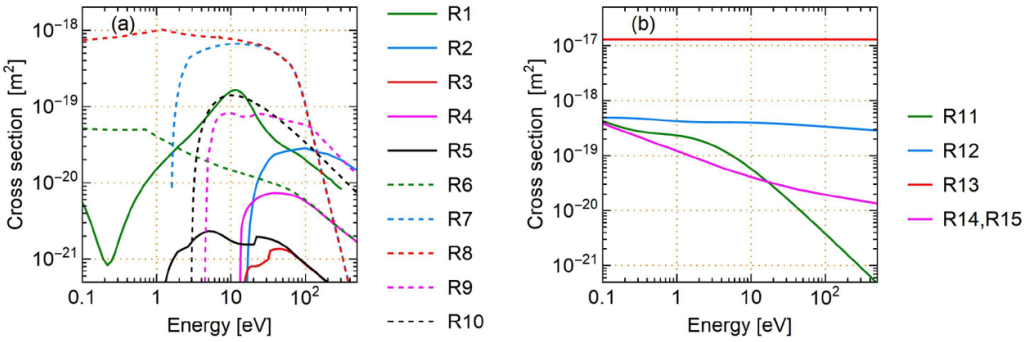


**Figure 1.** (a) Cross sections for electron-neutral collisions (reactions (1)–(10)) and (b) ion-neutral/neutral-neutral collisions (reactions (11)–(15)).

we briefly discuss the applicability of one-dimensional simulations in describing the real magnetized CCP discharges by estimating the plasma losses in different directions. We assume the one-dimensional PIC simulations are applied to discharge devices with a closed azimuthal $\boldsymbol{E}\times\boldsymbol{B}$ drift (e.g. RF magnetron sputtering and RF plasma thrusters), for this drift loss can be ignored in such structures. For case 3 at 60 G, parallel to the electric field, the calculated time-averaged particle flux (for both electrons and argon ions) on the electrode is about $\Gamma_E = 4\times10^{18}$ m$^2$s$^{-1}$. On the other hand, we use the Bohm velocity $u_B$ to estimate the particle flux leaving the bulk plasma in the direction parallel to the magnetic field and obtain the spatiotemporally-averaged particle flux of $\Gamma_B = \langle n\cdot u_B\rangle \approx 2.1\times10^{19}$ m$^2$s$^{-1}$. Therefore, the plasma losses parallel to the electric field and parallel to the magnetic field is approximately equal when the ratio of the electrode area $A_e$ to the side area $A_s$ is about $R = A_e/A_s \approx 5$. For real magnetized CCP plasmas with a closed $\boldsymbol{E}\times\boldsymbol{B}$ drift, the discharge properties can be qualitatively described by the one-dimensional simulation when the aspect ratio $R$ is sufficiently large (e.g. significantly greater than 5 for a magnetic field of 60 G).

## 3. Results and discussions

The electron densities and temperatures at the center of the discharge were obtained under different magnetic fields, as shown in figure 2, for the afore-defined three cases with different reactions. In case 1, metastable atoms are not considered, the collisions include the electron-neutral elastic and ionization, as well as the isotropic and backscattering of heavy particles. Based on case 1, case 2 includes electron-impact excitation collisions, which is the most widely used reaction set for argon discharges [33–35]. Case 3 tracks metastable atoms as particles, and includes all the multistep and the metastable pooling reactions listed in table 1. The details of tracked species and adopted reactions can be found in table 2. The electron temperatures in eV are derived from the electron pressure tensor as $T_e = p_{e,xx}/n_e$ [35], where $p_{e,xx} = m_e n_e(\langle v_x^2\rangle - u_e^2)$ is the diagonal element of the pressure tensor, $m_e$ the electron mass, $n_e$ the electron density, $v_x$ the velocity of an individual electron in the $x$-direction, and $u_e$ the electron mean velocity.

As shown in figure 2(a), the electron density at the center of the discharge increases with the increase in the magnetic field for all cases, due to the enhanced confinement of electrons under higher magnetic fields. Comparing cases 1 and 2, by considering the electron-impact excitation reactions, the electron densities reduced by about 1.7 times in all magnetic fields, due to the additional electron energy loss through the electron-impact excitation. For case 3, which includes metastable atoms on the basis of case 2, the electron density is barely changed in the absence of a magnetic field. The little influence of metastable atoms on the discharge of unmagnetized RF plasmas at low pressures is consistent with the previous PIC simulations [12, 13]. However, with the increase in the magnetic field, the electron density increases significantly, even higher than case 1 at 60 G. The results provide direct evidence that metastable atoms play an important role in low pressure magnetized RF discharges. From figure 2(b), the electron temperature $T_e$ at the center of the discharge rises with increasing the magnetic field and peaks at about 2.5 eV. The increase of $T_e$ in the magnetic field range from 0 G to 20 G is consistent with the previous measurement [4, 36] and simulation [37] results. The increase of $T_e$ in the bulk plasma can be attributed to the enhanced heating of low-energy electrons at low pressures, as will be shown in figure 4. However, as further increasing the magnetic field from 20 G to 60 G, the electron temperature deviates from each other for different cases, albeit in all cases there is a downward trend. Case 2 has the smallest variation in $T_e$, which is similar to the previous simulation results using the similar reaction set [37]. For case 3, with the inclusion of metastable atoms, $T_e$ decreases significantly, which will be analyzed based on the EEPF in figure 4.

Figure 3 shows the electron density and temperature profiles at different magnetic fields for case 3. The electron density is always parabolic, peaks at the center of the discharge and decreases towards the electrodes, while the electron temperature peaks near the electrodes. Previous PIC simulations with a reaction set similar to case 2 [37] showed that the magnetic field larger than 20 G has little influence on the electron temperature. Similar $T_e$ profiles are observed in our simulations of case 2, i.e. with the increase in the magnetic field up to 30 G, the shape of $T_e$ profile changes from convex to flat, and remains nearly unchanged with further increase of the magnetic field (data not shown). However, as shown in figure 2(b)

**Table 1.** Reactions considered in the simulation of argon discharges.

| | Reaction | Reference |
|---|---|---|
| (1) | $e + Ar \rightarrow e + Ar$ | [23] |
| (2) | $e + Ar \rightarrow 2e + Ar^+$ | [24] |
| (3) | $e + Ar \rightarrow e + Ar(4s)$ | [25] |
| (4) | $e + Ar \rightarrow e + Ar(4p)$ | [25] |
| (5) | $e + Ar(4s) \rightarrow e + Ar$ | [25] |
| (6) | $e + Ar(4p) \rightarrow e + Ar$ | [25] |
| (7) | $e + Ar(4s) \rightarrow e + Ar(4p)$ | [26] |
| (8) | $e + Ar(4p) \rightarrow e + Ar(4s)$ | [27] |
| (9) | $e + Ar(4s) \rightarrow 2e + Ar^+$ | [28] |
| (10) | $e + Ar(4p) \rightarrow 2e + Ar^+$ | [29] |
| (11) | $Ar^+ + Ar \rightarrow Ar^+ + Ar$ | [30] |
| (12) | $Ar^+ + Ar \rightarrow Ar + Ar^+$ | [30] |
| (13) | $Ar(4s) + Ar(4s) \rightarrow e + Ar^+ + Ar$ | [31] |
| (14) | $Ar(4s) + Ar \rightarrow Ar(4s) + Ar$ | [32] |
| (15) | $Ar(4p) + Ar \rightarrow Ar(4p) + Ar$ | [32] |

**Table 2.** Tracked species and adopted reactions for each case (1–3).

| | Tracked species | Adopted reactions |
|---|---|---|
| Case 1 | e, $Ar^+$ | 1, 2, 11, 12 |
| Case 2 | e, $Ar^+$ | 1–4, 11, 12 |
| Case 3 | e, $Ar^+$, Ar(4s), Ar(4p) | 1–15 |

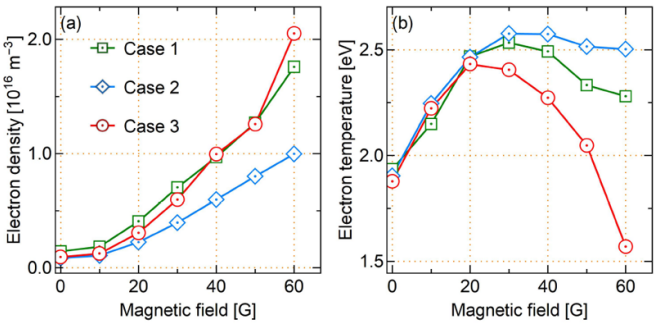


**Figure 2.** (a) The electron density and (b) the electron temperature versus transverse magnetic fields at the center of the discharge for case 1: without metastable atoms (reactions (1), (2), (11), and (12)), case 2: with electron-impact excitation to metastable atoms (reactions (1)–(4), (11), and (12)), case 3: with metastable atoms and all reactions (1)–(15).

and figure 3(b), with the inclusion of metastable atoms and related reactions, the electron temperature at the center of the discharge reduces significantly at higher magnetic fields.

The EEPFs are also calculated and shown in figure 4, which depicts the electron kinetics in RF discharge with the magnetic field. It demonstrates the EEPFs at the center of the discharge at various magnetic fields for the three cases. For all cases at 0 G, a bi-Maxwellian distribution is observed, which is typical in low pressure discharges and is in agreement with the experimental measurements [38] and other PIC simulations [12, 34]. With the increase in the magnetic field from 0 G to 20 G, a transition from bi-Maxwellian type to Druyvesteyn type is observed for all cases, corresponding to the consistence in $T_e$ from 0 G to 20 G for all cases in figure 2(b). This variation in

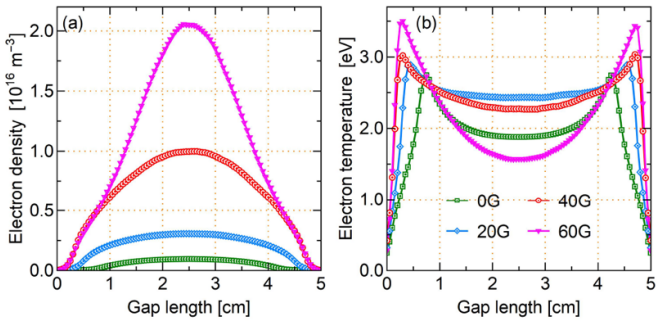


**Figure 3.** Time-averaged spatial profiles of (a) electron density and (b) electron temperature of case 3 for different magnetic fields.

EEPF with the magnetic field is consistent with previous PIC simulations as well [37]. Comparing cases 1 and 2, when the electron-impact excitation collisions are included, due to their maximum collision cross section at an electron energy of 35 to 50 eV [25], a large number of mid-energy (lower than 30 eV) electrons are produced, resulting in a higher $T_e$ at high magnetic fields as shown in figure 2(b). For case 3, with the inclusion of metastable atoms, the EEPF at 0 G is barely influenced, which is expected, since the dominant ionization mechanism at low pressures is the electron-impact ionization from ground state [12]. At higher magnetic fields, the discharge operates in local regime instead of nonlocal regime [36], the energetic electrons from the near-electrode region have little contribution to the center of the discharge. Therefore, after considering the multistep ionization with a lower energy threshold, the mid-energy electrons at the center of the discharge react sufficiently with the metastable atoms, resulting in a significant reduction in mid-energy electrons as well as in electron temperature. The influence of magnetic fields on discharges is similar to the influence of pressures, that the EEPF is typically concave at low pressures and convex at high pressures, with a transition at around a few hundred mTorr [34, 38, 39]. Under relatively high pressures, when the multistep ionization becomes important, neglecting the metastable atoms can result in a deviation of calculated EEPF from the measurement [40, 41]. Here we show that the neglecting of metastable atoms under high magnetic fields and low pressures can as well result in significant deviations.

Figure 5 shows the time-averaged spatial profiles of the ionization rates at different magnetic fields for case 3. The contribution to ionization can be divided into three parts, i.e. the ground state ionization (collisions between electron and ground state Ar), the multistep ionization (collisions between electron and metastables, i.e. Ar(4s) and Ar(4p)), and the metastable pooling (collisions between Ar(4s) particles). In the absence of a magnetic field, the ionization is primarily due to the direct ionization from ground state, which is 2 to 3 orders of magnitude larger than the other processes. The second primary mechanism is the multistep ionization from Ar(4p). The ionization from Ar(4s) and the metastable pooling are always negligible under all magnetic fields. From figure 5(a), the metastable atoms have little influence on the discharge characteristics, the dominant ionization mechanism

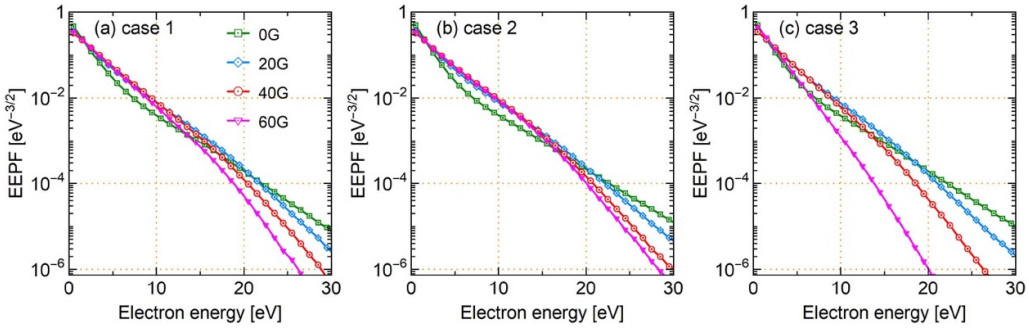


**Figure 4.** Time-averaged electron energy probability functions at the center of the discharge for different magnetic fields for (a) case 1, (b) case 2, and (c) case 3.

in low pressure RF discharges is the direct ionization from ground state, which is consistent with the previous PIC simulations [12, 13]. The profiles of all ionization rates at 0 G are relatively uniform across the bulk plasma region, since the discharge operates in nonlocal regime and the mean free path of electrons is much larger than the gap length. With the increase in the magnetic field, energetic electrons that gain energy by interacting with the oscillating sheaths are trapped, resulting in off-centered peaks in the profiles of ionization rate from the ground state. At 60 G, at the center of the discharge, the ionization rate from the ground state is even lower than the multistep ionization from Ar(4p), due to the lower threshold energy of multistep ionization and the reduced electron temperature at the center. The multistep ionization rates in the bulk plasma increases by about one order of magnitude with the increase in the magnetic field from 0 G to 20 G, and slightly decreases as further increasing the magnetic field. This is the same trend as the electron temperature (see figure 2(b)), which means that the multistep ionization is primarily modulated by the electron temperature. The profiles of multistep ionization are quite uniform comparing with the direct ionization from ground state, since the multistep ionization is carried out predominantly by the lower energy bulk electrons. The rates of direct ionization from ground state of case 2 are provided as well to illustrate the influence of metastable atoms on the ionization rates. From figure 5(a)–(d), the increased deviation in direct ionization rate at the center at high magnetic fields can be attributed to the locally reduced electron temperature. According to the Einstein relation [1], the diffusion coefficient, proportional to $T_e$, is much reduced at the center of the discharge after considering metastable atoms in the simulation. The inclusion of metastable atoms results in a reduction in both the diffusion loss and the total ionization rate, with the former decreasing more than the latter. Therefore, a higher electron density is achieved at the center at high magnetic fields by including the metastable atoms.

Figures 6(a) and (b) demonstrate the spatial density profiles of metastable atoms Ar(4s) and Ar(4p) under different magnetic fields for case 3. With the increase in the magnetic field, the metastable profiles change their shapes from a parabolic type under weak magnetic fields, to a flat type distribution for Ar(4s) and a saddle type distribution for Ar(4p) at higher magnetic fields. The transition of metastable density

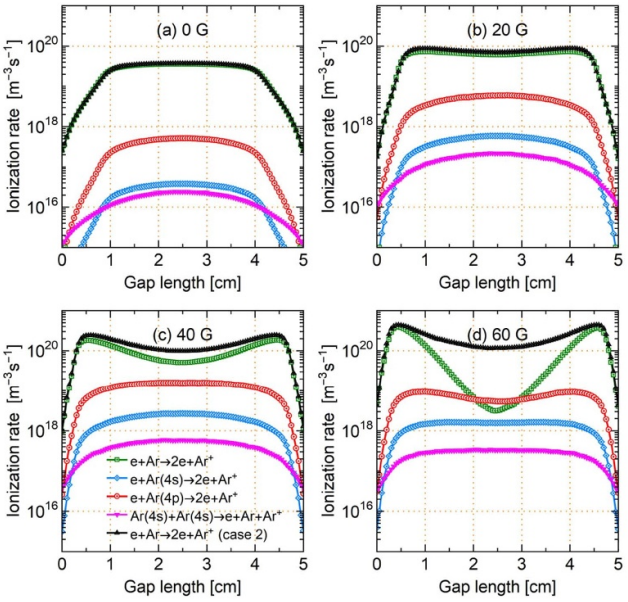


**Figure 5.** Time-averaged spatial profiles of ionization rates at (a) 0 G, (b) 20 G, (c) 40 G, and (d) 60 G for case 3.

profiles from parabolic to saddle type has been observed in RF argon discharges with the increase in the working pressure [12, 13, 42], the driving voltage [10, 43], or the discharge frequency [21, 43]. However, the variation of the maximum density is commonly monotonous, i.e. the metastable density increases with the controlling parameter at all locations between the electrodes. This is different from our situation. As shown in figure 6(c), the number density at the center of the discharge peaks at around 30 G to 40 G with the increase in the magnetic field, for both Ar(4s) and Ar(4p). At 60 G, the Ar(4p) density at the center is even lower than that in the absence of magnetic fields. The profiles of Ar(4p) roughly follow the profiles of electron temperature, which means that the modulation of the electron temperature plays an important role in the production and loss of metastable atoms.

Figure 7 shows the production and loss rates of Ar(4p) for case 3. From figures 7(a)–(c), the primary production mechanism at lower magnetic field is the electron-impact excitation

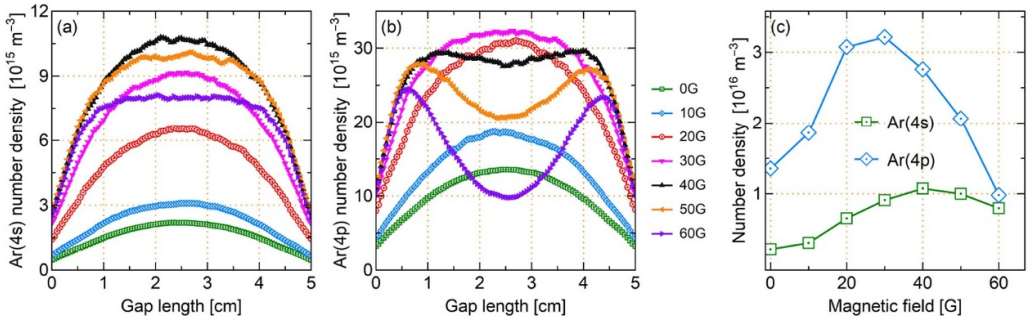


**Figure 6.** Time-averaged spatial density profiles of (a) Ar(4s), and (b) Ar(4p) under different magnetic fields for case 3, and (c) their corresponding values at the center of the discharge.

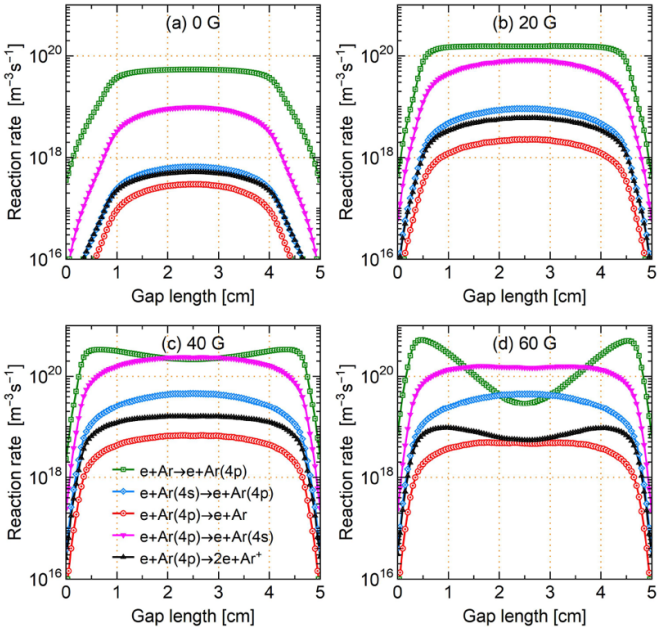


**Figure 7.** Time-averaged spatial profiles of Ar(4p)-related reaction rates at (a) 0 G, (b) 20 G, (c) 40 G, and (d) 60 G for case 3.

from ground state. The partial de-excitation to Ar(4s) is the dominant loss process of Ar(4p). At 60 G, further excitation from Ar(4s) becomes the primary production mechanism at the center of the discharge, due to the much lower threshold energy and the reduced electron temperature at the center. At higher magnetic fields, a convex shape of Ar(4p) density profiles appears at the center of the discharge, as shown in figure 6(b), due to the local production rate being less than the loss rate.

## 4. Conclusions

In summary, one-dimensional particle-in-cell/Monte Carlo collision simulations are performed to investigate the effects of metastable atoms on low pressure magnetized capacitively coupled argon discharges. Three cases are performed, namely, without considering metastable atoms, without metastable atoms but considering the electron energy loss through electron-impact excitation reactions, and tracking metastable atoms as particles and considering all related reactions. The magnetic field is varied from 0 G to 60 G, for a constant discharge voltage of 100 V and a constant driving frequency of 15 MHz, at a fixed pressure of 10 mTorr and a fixed electrode separation of 5 cm.

Two metastable levels of argon, i.e. Ar(4s) and Ar(4p) are included and tracked as particles, makes it possible to investigate the influence of multistep ionization and metastable pooling. The metastable argon atoms have little influence on low pressure, unmagnetized discharges. However, at higher magnetic fields up to 60 G, the electron density increases and the electron temperature decreases at the center of the discharge with the inclusion of metastable atoms. At high magnetic fields, the discharge operates in local regime instead of non-local regime, the energetic electrons from the near-electrode region have little contribution to the center of the discharge. Since the threshold energy of multistep ionization is much lower than that of direct ionization, with the inclusion of metastable atoms, the mid-energy electrons at the center of the discharge react sufficiently with the metastable atoms, resulting in a significant reduction in mid-energy electrons as well as in electron temperature.

The reduction in electron temperature at the center of the discharge has two opposite effects on the electron density. On the one hand, the low electron temperature leads to a reduction in the total ionization rate. On the other hand, the diffusion of plasma is suppressed at low electron temperatures. Therefore, we may speculate that the increase in electron density at the center of the discharge may be due in part to the reduction in diffusion loss and in part to the distortion in the ionization rate profile. The shape of metastable density profiles changes from parabolic to saddle type with the increase in the magnetic field, primarily modulated by the electron temperature. Metastable atoms may play an important role in the discharge of low pressure, magnetized plasmas, which should be considered in the simulation. Future work will include the influence of metastable species in more complicated discharges, such as electronegative discharges.

## Acknowledgment

This work is partly supported by the National Science Foundation Award Nos. 1917577, 1724941, and 1700787.

## ORCID iDs

Bocong Zheng https://orcid.org/0000-0002-6052-3693
Yangyang Fu https://orcid.org/0000-0001-9593-3177

## References

[1] Lieberman M A and Lichtenberg A J 2005 *Principles of Plasma Discharges and Materials Processing* (Hoboken, NJ: Wiley)
[2] Mattox D M 2010 *Handbook of Physical Vapor Deposition (PVD) Processing* (Burlington, MA: William Andrew)
[3] Kushner M J 2003 *J. Appl. Phys.* **94** 1436
[4] Turner M M, Hutchinson D A W, Doyle R A and Hopkins M B 1996 *Phys. Rev. Lett.* **76** 2069
[5] Zheng B, Wang K, Grotjohn T, Schuelke T and Fan Q H 2019 *Plasma Sources Sci. Technol.* **28** 09LT03
[6] Hutchinson D, Turner M, Doyle R and Hopkins M 1995 *IEEE Trans. Plasma Sci.* **23** 636
[7] Yang S, Zhang Y, Wang H-Y, Wang S and Jiang W 2017 *Phys. Plasmas* **24** 033504
[8] Adamovich I *et al* 2017 *J. Phys. D: Appl. Phys.* **50** 323001
[9] Korolov I *et al* 2020 *J. Phys. D: Appl. Phys.* **53** 185201
[10] Lymberopoulos D P and Economou D J 1993a *J. Appl. Phys.* **73** 3668
[11] Lymberopoulos D and Economou D 1995 *J. Res. Natl Inst. Stand. Technol.* **100** 473
[12] Roberto M, Smith H and Verboncoeur J 2003 *IEEE Trans. Plasma Sci.* **31** 1292
[13] Lauro-Taroni L, Turner M M and Braithwaite N S 2004 *J. Phys. D: Appl. Phys.* **37** 2216
[14] Anders A 2017 *J. Appl. Phys.* **121** 171101
[15] Scheller G R, Gottscho R A, Graves D B and Intrator T 1988 *J. Appl. Phys.* **64** 598
[16] Lymberopoulos D P and Economou D J 1993b *Appl. Phys. Lett.* **63** 2478
[17] Sansonnens L, Howling A A, Hollenstein C, Dorier J L and Kroll U 1994 *J. Phys. D: Appl. Phys.* **27** 1406
[18] Rauf S and Kushner M J 1997 *J. Appl. Phys.* **82** 2805
[19] Hebner G A, Barnat E V, Miller P A, Paterson A M and Holland J P 2006 *Plasma Sources Sci. Technol.* **15** 879
[20] Ishimaru M, Ohba T, Ohmori T, Yagisawa T, Kitajima T and Makabe T 2008 *Appl. Phys. Lett.* **92** 071501
[21] Sharma S, Sirse N, Turner M M and Ellingboe A R 2018 *Phys. Plasmas* **25** 063501
[22] Gudmundsson J T, Kawamura E and Lieberman M A 2013 *Plasma Sources Sci. Technol.* **22** 035011
[23] Zatsarinny O and Bartschat K 2004 *J. Phys. B: At. Mol. Opt. Phys.* **37** 4693
[24] Yamabe C, Buckman S J and Phelps A V 1983 *Phys. Rev.* A **27** 1345
[25] Tachibana K 1986 *Phys. Rev.* A **34** 1007
[26] Zapesochnyi I, Shimon L and Soshnikov A 1965 *Opt. Spectrosc.* **19** 480
[27] Zapesochnyi I, Semenyuk Y N, Dashchenko A, Imre A and Zapesochnyi A 1984 *JETP Lett.* **39**
[28] McFarland R H and Kinney J D 1965 *Phys. Rev.* **137** A1058
[29] Vriens L 1964 *Phys. Lett.* **8** 260
[30] Phelps A V 1994 *J. Appl. Phys.* **76** 747
[31] Okada T and Sugawara M 1996 *Japan. J. Appl. Phys.* **35** 4535
[32] Phelps A V 1991 *J. Phys. Chem. Ref. Data* **20** 557
[33] Vahedi V and Surendra M 1995 *Comput. Phys. Commun.* **87** 179
[34] Lafleur T, Chabert P and Booth J P 2014 *Plasma Sources Sci. Technol.* **23** 035010
[35] Schulze J, Donkó Z, Lafleur T, Wilczek S and Brinkmann R P 2018 *Plasma Sources Sci. Technol.* **27** 055010
[36] You S J and Chang H Y 2006 *Phys. Plasmas* **13** 043503
[37] Lee S H, You S J, Chang H Y and Lee J K 2007 *J. Vac. Sci. Technol.* A **25** 455
[38] Godyak V A and Piejak R B 1990 *Phys. Rev. Lett.* **65** 996
[39] Vahedi V, Birdsall C K, Lieberman M A, DiPeso G and Ronhlien T D 1993 *Plasma Sources Sci. Technol.* **2** 273
[40] Bohle A and Kortshagen U 1994 *Plasma Sources Sci. Technol.* **3** 80
[41] Heil B G, Brinkmann R P and Czarnetzki U 2008 *J. Phys. D: Appl. Phys.* **41** 225208
[42] McMillin B K and Zachariah M R 1995 *J. Appl. Phys.* **77** 5538
[43] Zhang Y-R, Xu X and Wang Y-N 2010 *Phys. Plasmas* **17** 033507